Physicochemical Properties Important for Carbon Dioxide Absorption in Aqueous Methyldiethanolamine

Hani A. Al-Ghawas, Daniel P. Hagewiesche, Gabriel Ruiz-Ibanez, and Orville C. Sandall*

Department of Chemical and Nuclear Engineering, University of California, Santa Barbara, Santa Barbara, California 93106

The objective of this work is to experimentally determine the diffusion coefficient and free-gas solubility of carbon dioxide in aqueous methyldiethanolamine (MDEA). Solution viscosity and density were also measured. Experiments covered the concentration range 0-50 wt % MDEA for temperatures between 15 and 50 °C. Since the solubility and diffusivity of a gas cannot be measured directly in a system in which it reacts, the N_2O analogy method was used in this work to estimate these properties for the system CO_2-aqueous MDEA solutions. Solubilities were measured volumetrically in an equilibrium cell, and diffusion coefficients were measured in a laminar liquid jet absorber for low MDEA concentrations and a wetted-sphere absorber for high MDEA concentrations. Properties were correlated by convenient equations which were found to be in excellent agreement with the experimental data.

Introduction

The objective of this research is to experimentally determine physical properties important for the absorption of CO_2 into aqueous methyldiethanolamine (MDEA) solutions. The properties measured are useful for the experimentalist or the process design engineer who is interested in the problem of acid gas removal using aqueous MDEA.

In industrial treatment of acid gas streams, it is often desirable to separate sulfur gases from CO_2. In recent years, most of the research on selective H_2S absorption has focused on sterically hindered amines and in particular tertiary amines. It is the inability of tertiary amines to form carbamates by reaction with CO_2 that provides a much slower reaction than that of primary and secondary amines. MDEA, a tertiary amine, was found to provide the necessary kinetic selectivity to separate H_2S from CO_2 as illustrated by the study of Haimour et al. (*1*). Industrial development of the MDEA process did not take place until the 1970s. Vidaurri and Kahre (*2*) used bench, pilot, and commercial plants to study the selectivities of MDEA, triethanolamine (TEA), diglycolamine (DGA), monoethanolamine (MEA), and diethanolamine (DEA). Their conclusion was that MDEA was the most efficient, and the best results were achieved when the absorber was operated at high solvent loading and short contact times. Pearce and Brownlie (*3*) observed that amine compounds having an alkyl-substituted nitrogen offer the highest selectivity for H_2S. They also noticed that the base strength of the compound largely determines the acid gas capacity and rate of reaction. The ability of these compounds to selectively absorb H_2S increases with an increase in the number of nitrogen alkyl substitutions and with an increase in the side chain length that is attached to the substituted nitrogen. Pearce and Brownlie (*3*) concluded that among the amines tested MDEA had the best overall balance of desirable characteristics for a selective reactive absorbent for the treatment of acid gases. Goar (*4*) and Daviet et al. (*5*) have reported improved performance of an amine gas-treating plant when MDEA is substituted for other amine solvents and they describe several gas-treating schemes using MDEA.

CO_2 solubility and diffusivity are needed to analyze the experimental absorption data in order to determine the reaction kinetics with MDEA or to be used in models for predicting the gas absorption rate. These properties, however, cannot always be measured directly by experimental methods because the gas undergoes a chemical reaction with the solvent. The similarity in mass, molecular structure, and molecular interaction parameters between CO_2 and N_2O led Clarke (*6*) to assume that the ratios of the solubilities or diffusivities of CO_2 and N_2O in water and in aqueous solutions of organic solvents is similar within 5% or better at the same temperature. That is, the ratios D_{CO_2}/D_{N_2O} and H_{CO_2}/H_{N_2O} in water and in solutions having different amine concentrations are assumed to be constant at constant temperature. This method was later used by Weiland and Trass (*7*), Joosten and Danckwerts (*8*), Sada et al. (*9*, *10*), Alvarez-Fuster et al. (*11*, *12*), Laddha et al. (*13*), and Haimour and Sandall (*14*) to estimate these parameters for CO_2 in various amine solutions. Haimour and Sandall (*14*) experimentally verified that the N_2O analogy holds for estimating the solubility and diffusivity of CO_2 in aqueous MDEA solutions. Al-Ghawas et al. (*15*) reported that the N_2O analogy can also be used to estimate the solubility and diffusivity of COS in aqueous MDEA.

The data reported here extend the range in MDEA concentration and temperature for the solubility and diffusivity measurements of CO_2 in aqueous MDEA solutions reported by Haimour and Sandall (*14*).

Experimental Section

Amine solutions were prepared from deionized, distilled water and MDEA having a purity of 99+% obtained from Union Carbide. Water and MDEA were mixed in 20-L Pyrex bottles, and degassed by heating while the solution was under vacuum. The amine concentration was checked by titration against 1 M HCl to a pH of 4.5 for the equivalence point. The concentrations are accurate to within 0.5 wt %.

Density. The densities of aqueous amine solutions and of the pure components over the temperature range 15-60 °C were determined by using a 49.447-mL (at 25 °C) Gay-Lussac pycnometer. The experimental method was in accordance with the ASTM D3505 standard test method. The bath temperature was controlled within ±0.05 °C of the test temperature. Calibration runs were made using pure degassed water at 25 °C. These measurements were compared with data reported by Perry and Chilton (*16*). The experimental measurements were accurate to within ±0.05%.

Viscosity. The kinematic viscosity of aqueous MDEA solutions containing 10-50 wt % amine and of pure MDEA were measured over the temperature range 15-60 °C by using a Cannon-Fenske routine viscometer for transparent liquids. These measurements were done according to the specifications and operating instructions of the ASTM D446 standard test method. The bath temperature was controlled within ±0.05 °C of the test temperature. The calibration of the viscometers, required by the method, was done with pure degassed water using the data reported by West (*17*) and with pure MDEA using

* Author to whom correspondence should be addressed.

0021-9568/89/1734-0385$01.50/0

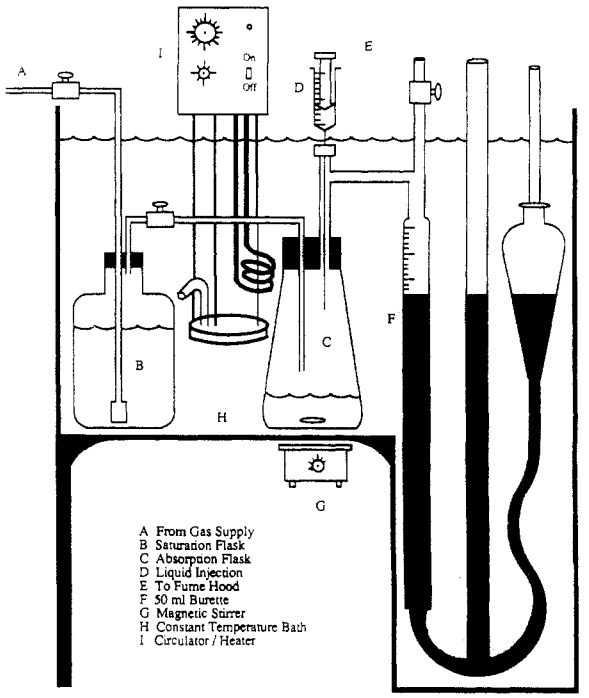

Figure 1. Schematic drawing of solubility apparatus.

the data reported in the "Product Information Sheet" by Union Carbide Corporation. The experimental measurements agreed with the reported values within a mean deviation of 3.6%.

The dynamic viscosity μ was then calculated from

$$\mu = \rho\nu \tag{1}$$

where ρ is the density of the solution at the same temperature and ν its kinematic viscosity.

Solubility. Henry's law can be applied to relate the equilibrium concentration of the gas in a liquid as a function of its partial pressure in the gas phase. Solubility is defined in different ways, but the definition used here is

$$H_A = p_A/C^*_A \tag{2}$$

where C^*_A is the equilibrium concentration of the gas which can be calculated from the total moles of gas physically absorbed in a volume of absorbing liquid.

The solubility of N_2O in water and in MDEA solutions was measured by using the apparatus shown schematically in Figure 1. This apparatus is a modified version of the apparatus used by Haimour and Sandall (*14*). The principle idea of this method is to bring a known volume of liquid into contact with a gas in a closed system at constant temperature and pressure. Equilibrium is reached by agitating the liquid for some time until no change in the volume of the gas is observed. The amount of gas absorbed is measured volumetrically.

The procedure for making a solubility measurement is as follows. A gas saturated with the vapors of the adsorbing liquid is passed through the system at constant temperature long enough to completely purge the absorption flask. Then the inlet and outlet valves are closed. The height of the mercury in the three branches is leveled, ensuring that the pressure in the flask is atmospheric, and the position of the meniscus is recorded. An aliquot of degassed liquid which was kept at the same temperature of the experiment is weighed and then injected into the absorption flask. The liquid sample is continuously agitated via an external magnetic stirrer. The height of the mercury in the three branches is leveled every few minutes to make sure that the gas phase is at atmospheric pressure. Equilibrium is reached when the height of the mercury in each branch is leveled and remains constant. The measured volume change is equal to the volume of liquid sample minus the volume of the gas absorbed. The whole apparatus is kept at constant temperature inside a temperature-controlled bath. The bath temperature variation is less than 0.2 °C during any given run. The partial pressure of the gas in eq 2 is obtained from the measured total pressure corrected for water vapor pressure as calculated from

$$p^{vap}_{H_2O} = 1.35337 \times 10^6 \exp(-5243.04/T) \tag{3}$$

Equation 3 was obtained by fitting vapor pressure data given by Perry and Chilton (*16*) and West (*17*) over the temperature range of interest.

In order to verify proper operation of the apparatus, the solubility of the well established system N_2O–water was measured and compared with the values reported by the International Critical Tables (*18*). The estimated experimental error in all solubility measurements was less than 2%.

In this work the solubility of N_2O in aqueous MDEA solutions over the composition range 0–50 wt % and temperature range 15–50 °C was measured. To interpret these data, the partial pressure of N_2O in eq 2 was corrected for solution vapor pressure by use of Raoult's law.

After the solubility of N_2O in the solutions of interest was measured experimentally, CO_2 solubility was estimated by using the N_2O analogy given by

$$H_{CO_2} = H_{N_2O}(H^\circ_{CO_2}/H^\circ_{N_2O}) \tag{4}$$

The solubility of CO_2 in pure water, $H^\circ_{CO_2}$, was taken from the International Critical Tables (*18*).

Diffusivity. The analogy between N_2O and CO_2 was used to estimate the molecular diffusivity of CO_2 in MDEA solutions of various compositions. The molecular diffusivity of a solute gas in a liquid can be measured directly only when gas and liquid do not react. It is not possible, in general, to directly measure this property when the gas chemically reacts with the absorbing liquid.

Two contact devices that are commonly used in gas absorption studies are the laminar liquid jet apparatus and the wetted-sphere apparatus. The ranges of operational contact times for these devices are 0.001–0.02 and 0.1–1.0 s, respectively. The laminar liquid jet apparatus was used to measure the diffusion coefficients of N_2O in water and in 10 and 20 wt % MDEA solutions. For the 30 wt % MDEA solution the absorption rates of N_2O using the jet apparatus were very small, a condition that made the experimental error too significant to ignore. This effect was due to the short contact times available in the jet apparatus and to the low solubility of N_2O in solutions of high amine content. For this reason the diffusion coefficients of N_2O in 30–50 wt % MDEA solutions were measured by using the wetted-sphere apparatus.

Laminar Jet Apparatus. According to the penetration theory, the rate of absorption is given by

$$R_A = 4C^*_A (D_A hL)^{1/2} \tag{5}$$

Thus a plot of R_A versus $(hL)^{1/2}$ at constant temperature and pressure should give a straight line that passes through the origin and has a slope equal to $4C^*_A (D_A)^{1/2}$.

The laminar liquid jet apparatus used in this study is shown in Figure 2. The absorption chamber is made of a 31-cm-long, 7.6-cm-i.d. Pyrex glass cylinder and is enclosed by a constant-temperature jacket constructed from a 31-cm-long, 16.5-cm-i.d. Pyrex glass cylinder. Both cylinders are held between two stainless steel flanges, and the ends are sealed with Teflon gaskets. Water to the jacket is supplied from and recycled to a constant-temperature circulating bath.

The liquid feed is pumped to a surge tank and then through a rotameter and through a coil in the constant-temperature

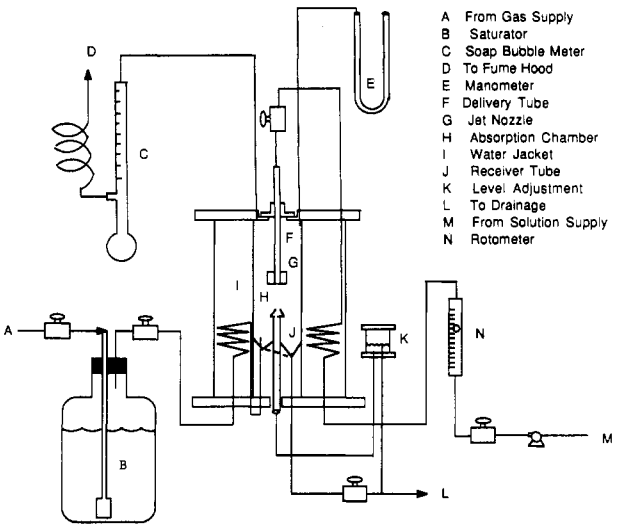

Figure 2. Schematic drawing of laminar liquid jet absorber.

jacket. It is then fed to a 1-cm-i.d. delivery glass tube. The surge tank which is topped by a closed space of nitrogen gas helps in eliminating pump pulses. The delivery glass tube can slide in the vertical direction and can be locked in position by a swage-lock nut with Teflon ferrules. The gas supply is fed to a saturator and then through a coil in the constant-temperature jacket. It is then introduced into the absorption chamber at the base and is exhausted at the top of the chamber. The exhaust line is connected to a soap film meter backward so that when the gas inlet is closed the gas retrieved to the chamber would flow through the soap film meter in the forward direction.

The jet nozzle assembly is fitted onto the end of the glass delivery tube by three O-rings. The jet nozzle is a square-edged orifice, 0.051 cm in diameter, drilled in a 0.008-cm-thick stainless steel sheet. This nozzle design was recommended by Raimondi and Toor (*19*) for absorption rate results closest to the theoretical values for rodlike flow and no interfacial resistance. The receiver is 1-cm-i.d. glass tube fitted into a funnel-shaped base and is capped by a Teflon plug in which a 0.1-cm hole is drilled. A hole in the base allows draining of any liquid overflow. The jet is centered by manipulating the mount of the delivery tube relative to the top flange. The jet is considered centered when all of its contents empty into the receiver with no overflow.

A leveling device consisting of a cup with an overflow drain is used to precisely adjust the liquid level in the receiver tube. If the level is low, gas entrainment occurs; if it is high, then the liquid overflows. The liquid level has to be readjusted after any changes in the liquid flow rate. The length of the jet is measured by a cathetometer with an error less than 0.5×10^{-2} cm.

The temperature of the system is monitored by thermometers in the constant-temperature jacket, in the jet chamber, and in the liquid delivery tube. The temperatures are controlled to within ±0.30 °C.

After the jet is flowing satisfactorily, the gas is turned on for enough time for the jet chamber and all the tubing to fill with the gas. Then the gas is turned off; the rate of gas absorption is found by measuring the amount of time needed for a soap film to travel through a certain volume.

All of the experiments were done under atmospheric pressure. The liquid flow rate varied between 0.25 and 1 mL/s, and the exposure time varied approximately between 0.001 and 0.015 s.

The apparatus and the experimental technique were tested by carrying out some initial experiments with the well-known system CO_2–water. These results are summarized in Table I, from which an average value of the diffusion coefficient of CO_2 in water at 25 °C is calculated as 1.95×10^{-5} cm²/s. This

Table I. Experimental Data and Diffusivity for Absorption of CO_2 in Water at 25 °C and 1 atm[a]

T, °C	h, cm	L, cm³/s	$10^7 R_A$, mol/s	$10^5 D_A$, cm²/s
25	2.737	0.62	7.570	1.95
25	2.737	1.015	9.711	1.96
25	2.737	1.40	11.317	1.93
25	1.221	0.62	5.030	1.93
25	1.221	1.015	6.601	2.03
25	1.931	0.62	6.391	1.97
25	1.931	1.015	8.260	2.01
25	1.054	0.62	4.625	1.89
25	1.054	1.015	5.995	1.94
25	1.428	0.62	5.355	1.87
25	1.428	1.015	6.996	1.95

[a] $C^*_A = 3.29 \times 10^{-5}$ mol/cm³.

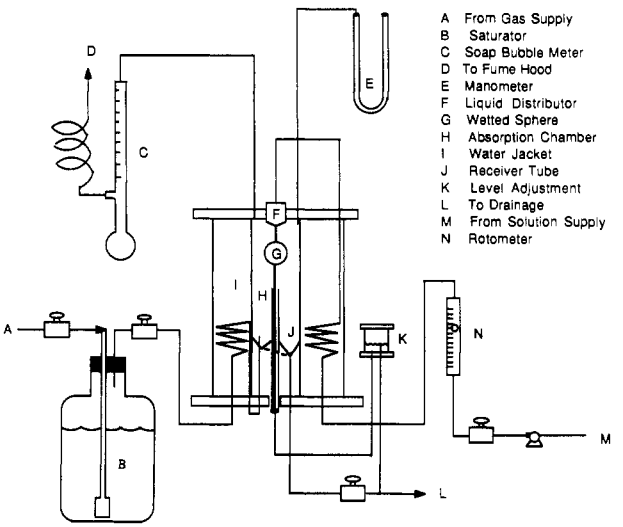

Figure 3. Schematic drawing of wetted-sphere absorber.

value shows good agreement with values available in the literature (*14*, *20*–*24*). The diffusivity of N_2O in water and in 10 and 20 wt % MDEA solutions was calculated from eq 5 or by plotting R_A versus $(hL)^{1/2}$.

Wetted-Sphere Apparatus. Davidson and Cullen (*25*) presented a solution for the problem of physical gas absorption by a laminar film flowing over a sphere. For small depth of penetration, the rate of absorption can be predicted by a series expansion of the form

$$R_A = L(C^*_A - C^\circ_A)\,[1 - \sum \beta_i \exp(-\gamma_i \alpha)] \qquad (6)$$

where

$$\alpha = 3.36\pi(2\pi g/3\nu)^{1/3} r_s^{7/3} L^{-4/3} D_A \qquad (7)$$

Olbrich and Wild (*26*) improved the general solution of Davidson and Cullen (*25*) by adding more terms to the series. Note that the value of γ_7 is misprinted in the paper by Olbrich and Wild (*26*). The correct value as calculated from their eq 19 is 461.8172.

The wetted-sphere apparatus used in this study is shown in Figure 3. The dimensions and construction materials of the apparatus are the same as those of the laminar jet apparatus, which was described earlier. The difference is the sphere assembly which is shown in Figure 3. The sphere, a Hastelloy ball of 3.76-cm diameter, was mounted on a 0.4-cm-diameter Hastelloy rod. The part of the rod above the sphere was accurately centered in the orifice of the liquid-feed distributor. This was achieved by axially mounting the rod onto a Teflon alignment block which, in turn, was a concentric tight fit in the liquid-feed distributor. The liquid feed enters at the top and passes through the alignment block via eight holes which en-

Table II. Measured Physical Properties for Pure Water

T, °C	ρ, g/mL	μ, cP	$H°_{N_2O}$, atm L/mol	$H°_{CO_2}$,[a] atm L/mol	$10^5 D°_{N_2O}$, cm^2/s	$10^5 D°_{CO_2}$,[b] cm^2/s
15	0.9991	1.138	28.59	22.11	1.285	1.50
20	0.9982	1.007	32.78	25.56	1.436	1.71
25	0.9970	0.895	38.59	29.45	1.569	1.93
30	0.9956	0.802	42.93	33.50	1.607	2.16
35	0.9940	0.724	46.49	37.60	1.634	2.42
40	0.9922	0.656	49.55	41.94	1.679	2.71
45	0.9902	0.596		46.28		3.01
50	0.9880	0.555	52.99	50.99	1.868	3.34
55	0.9857	0.504				
60	0.9832	0.476				

[a] International Critical Tables. [b] Reference 22.

Table III. Measured Physical Properties for 10 wt % MDEA Solution

T, °C	ρ, g/mL	μ, cP	H_{N_2O}, atm L/mol	H_{CO_2}, atm L/mol	$10^5 D_{N_2O}$, cm^2/s	$10^5 D_{CO_2}$, cm^2/s
15	1.0078	1.707	30.62	23.68	1.047	1.222
20	1.0069	1.477	34.51	26.91	1.158	1.379
25	1.0054	1.290	39.44	30.10	1.325	1.630
30	1.0040	1.137	44.24	34.52	1.432	1.925
35	1.0025	1.011	48.75	39.43	1.479	2.190
40	1.0007	0.907	51.37	43.48	1.611	2.600
45	0.9985					2.863
50	0.9960	0.748	54.90	52.83	1.764	3.154
55	0.9937					
60	0.9912	0.627				

sure even flow out of the orifice. After passing over the sphere, the liquid runs down a short length of rod into a 0.9-cm-i.d. receiving tube. The liquid is maintained at the top of this tube by a constant-level device.

The sphere is fixed at 0.3 cm from the liquid-feed orifice. This distance was chosen because at longer distances the liquid tended to break away from the rod and produced uneven distribution over the sphere. This condition is undesirable since it would alter the contact time and surface area by unpredictable amounts. At shorter distances, the liquid tended to spray out over the ball even at moderate flow rates. The length of rod between the sphere and the receiving tube was fixed at 2.0 cm, since it was found experimentally by Davidson and Cullen (*25*), Goettler (*27*), Wild and Potter (*28*), and Tomcej et al. (*29*) that for distances less than 2.0 cm the rate of adsorption drops appreciably owing to a "stagnant layer" end effect. When the distance was greater than 2.0 cm, "rippling" effects became significant.

Freshly degassed liquid is initially fed to the distributor at high flow rates to ensure complete wetting of the sphere. When the liquid film has stabilized, the flow rate is reduced to the desired rate. After the liquid film is flowing satisfactorily, the gas is turned on for enough time to purge the absorption chamber and for all the tubing to fill with the gas. The gas is then turned off, and the rate of gas absorption is found by measuring the amount of time needed for a soap film to travel through a fixed volume.

All of the experiments were done under atmospheric pressure. The liquid flow rates ranged between 0.15 and 1.7 mL/s, and the exposure time varied between approximately 0.2 and 0.6 s. The temperature of the system is monitored by thermometers in the constant-temperature jacket, in the absorption chamber, and in the liquid-feed distributor. The temperatures are controlled to within ±0.3 °C.

To test the experimental technique some initial experiments with CO_2 and water were carried out. The data were analyzed by using eq 6 and 7. The average value obtained for the diffusion coefficient of CO_2 in water at 25 °C was 1.94×10^{-5} cm^2/s. This value, in good agreement with values available in the literature (*14*, *20–24*), gives confidence in application of the penetration theory to the gas absorption dynamics obtained in the wetted-sphere apparatus.

Table IV. Measured Physical Properties for 20 wt % MDEA Solution

T, °C	ρ, g/mL	μ, cP	H_{N_2O}, atm L/mol	H_{CO_2}, atm L/mol	$10^5 D_{N_2O}$, cm^2/s	$10^5 D_{CO_2}$, cm^2/s
15	1.0180	2.650	32.30	24.98	0.841	0.982
20	1.0169	2.262	36.10	28.15	0.991	1.180
25	1.0152	1.941	42.33	32.30	1.148	1.412
30	1.0132	1.686	48.28	37.67	1.290	1.734
35	1.0113	1.474	51.04	41.28	1.412	2.091
40	1.0091	1.301	55.56	47.03	1.499	2.419
45						2.634
50	1.0047	1.051	57.65	55.47	1.670	2.986
55						
60	0.9993	0.858				

Table V. Measured Physical Properties for 30 wt % MDEA Solution

T, °C	ρ, g/mL	μ, cP	H_{N_2O}, atm L/mol	H_{CO_2}, atm L/mol	$10^5 D_{N_2O}$, cm^2/s	$10^5 D_{CO_2}$, cm^2/s
15	1.0290	4.402	36.06	27.89	0.712	0.831
20	1.0272	3.690	39.86	31.08	0.823	0.980
25	1.0250	3.092	45.05	34.38	0.973	1.197
30	1.0229	2.612	50.34	39.28	1.032	1.387
35	1.0205	2.250	53.06	42.91	1.162	1.721
40	1.0180	1.937	58.21	49.27	1.240	2.001
45					1.303	2.196
50	1.0130	1.505	59.95	57.68	1.421	2.541
55						
60	1.0069	1.207				

Table VI. Measured Physical Properties for 40 wt % MDEA Solution

T, °C	ρ, g/mL	μ, cP	H_{N_2O}, atm L/mol	H_{CO_2}, atm L/mol	$10^5 D_{N_2O}$, cm^2/s	$10^5 D_{CO_2}$, cm^2/s
15	1.0395	7.973	39.83	30.80	0.589	0.688
20	1.0371	6.452	42.92	33.49	0.639	0.761
25	1.0346	5.253	47.77	36.46	0.751	0.924
30	1.0322	4.359	53.58	41.81	0.824	1.108
35	1.0292	3.671	55.94	45.24	0.993	1.471
40	1.0266	3.112	61.25	51.84	1.108	1.788
45					1.174	1.979
50	1.0204	2.309	61.39	59.07	1.269	2.264
55						
60						

Table VII. Measured Physical Properties for 50 wt % MDEA Solution

T, °C	ρ, g/mL	μ, cP	H_{N_2O}, atm L/mol	H_{CO_2}, atm L/mol	$10^5 D_{N_2O}$, cm^2/s	$10^5 D_{CO_2}$, cm^2/s
15	1.0479	14.69	41.00	31.71	0.329	0.384
20	1.0454	11.70	45.56	35.53	0.430	0.512
25	1.0427	9.208	51.61	39.39	0.506	0.622
30	1.0396	7.436	55.57	43.36	0.561	0.754
35	1.0364	6.097	58.92	47.65	0.635	0.940
40	1.0331	5.105	63.42	53.68	0.752	1.214
45	1.0302				0.843	1.421
50	1.0269	3.642	62.87	60.50	0.933	1.688
55	1.0234					
60	1.0199	2.700				

The diffusivity of CO_2 in MDEA solutions at different temperatures can be estimated from the diffusivity of N_2O by means of the N_2O analogy given by

$$D_{CO_2} = D_{N_2O}(D°_{CO_2}/D°_{N_2O}) \quad (8)$$

The diffusivity of CO_2 in pure water, $D°_{CO_2}$, was obtained from

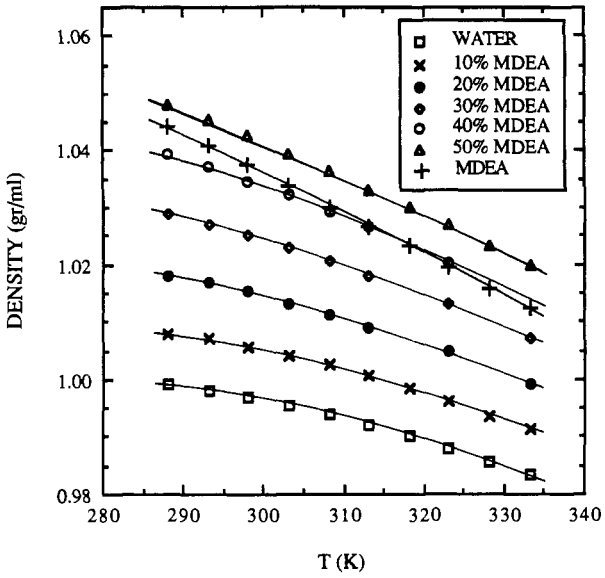

Figure 4. Experimental values of the density of aqueous MDEA as a function of temperature. Lines represent the correlation.

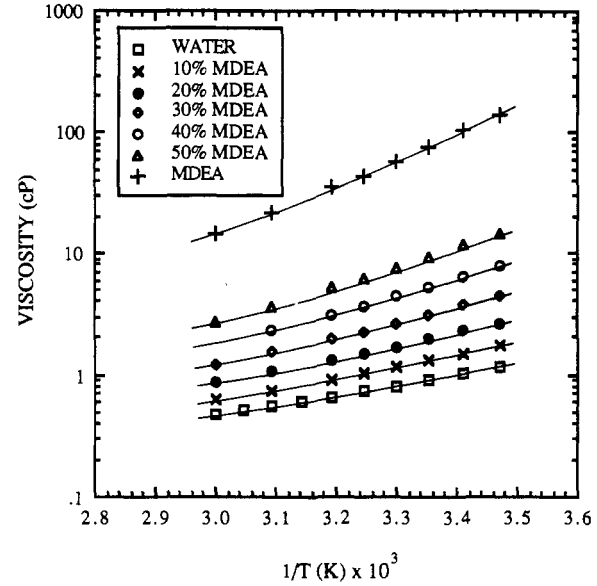

Figure 5. Experimental values of the viscosity of aqueous MDEA as a function of temperature. Lines represent the correlation.

Table VIII. Density and Viscosity of Pure MDEA

T, °C	ρ, g/mL	μ, cP	T, °C	ρ, g/mL	μ, cP
15	1.0445	141.9	40	1.0267	34.78
20	1.0410	104.5	45	1.0231	
25	1.0374	76.9	50	1.0194	21.98
30	1.0337	57.57	55	1.0158	
35	1.0302	44.14	60	1.0123	14.5

the data of Thomas and Adams (*22*).

Results and Correlations

The results of the experimental measurements for the physical properties important in the absorption of CO_2 into aqueous MDEA solutions are shown in Tables II–VIII and in Figures 4–7. The tables also show the values of H_{CO_2} and D_{CO_2} as estimated from the N_2O analogy and the values of $H^\circ_{CO_2}$ and $D^\circ_{CO_2}$ as taken from the International Critical Tables (*18*) and from Thomas and Adams (*22*), respectively.

The properties were correlated by convenient equations using the least-squares technique, where the temperature and MDEA mass fraction were used as the independent variables. The

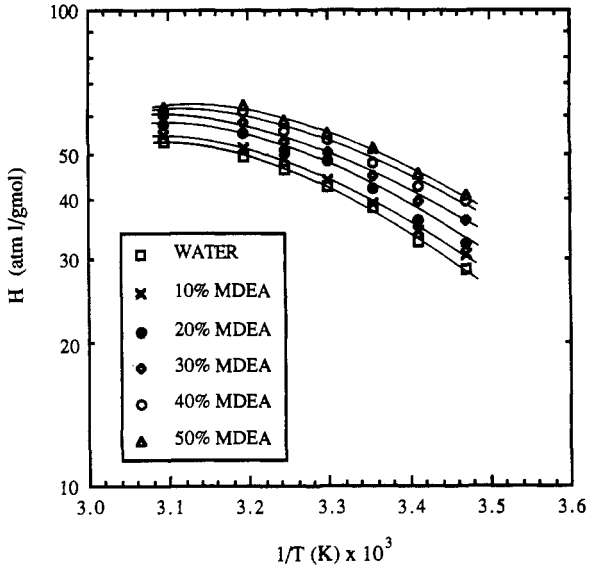

Figure 6. Solubility of nitrous oxide in aqueous MDEA. Lines represent the correlation.

Table IX. Coefficients for the Correlations According to Eq 17

	k_{ij}			
i/j	1	2	3	4
1	0.715 929	0.395 951	0.927 974	−0.794 931
2	$2.137\,99 \times 10^{-3}$	$-1.981\,73 \times 10^{-3}$	$-3.875\,53 \times 10^{-3}$	$3.042\,28 \times 10^{-3}$
3	$-4.009\,72 \times 10^{-6}$	$3.070\,38 \times 10^{-6}$	$3.584\,83 \times 10^{-6}$	$-2.709\,47 \times 10^{-6}$
4	$-1.952\,14 \times 10^{1}$	$-2.339\,79 \times 10^{1}$	$-3.123\,63 \times 10^{1}$	$3.617\,35 \times 10^{1}$
5	$3.912\,73 \times 10^{3}$	$4.858\,80 \times 10^{3}$	$8.477\,05 \times 10^{3}$	$-8.357\,76 \times 10^{3}$
6	$2.112\,2 \times 10^{-2}$	$3.338\,9 \times 10^{-2}$	$2.779\,8 \times 10^{-2}$	$-4.036\,7 \times 10^{-2}$
7	$-2.767\,08 \times 10^{1}$	$-2.518\,07 \times 10^{1}$	$2.949\,04 \times 10^{2}$	$-4.851\,83 \times 10^{2}$
8	$2.081\,56 \times 10^{4}$	$1.629\,30 \times 10^{4}$	$-1.866\,65 \times 10^{5}$	$3.033\,13 \times 10^{5}$
9	$-3.422\,41 \times 10^{6}$	$-2.593\,43 \times 10^{6}$	$2.957\,27 \times 10^{7}$	$-4.746\,32 \times 10^{7}$
10	2.018 74	$-2.376\,38 \times 10^{1}$	$2.900\,92 \times 10^{2}$	$-4.801\,96 \times 10^{2}$
11	$3.135\,49 \times 10^{3}$	$1.549\,31 \times 10^{4}$	$-1.839\,87 \times 10^{5}$	$3.005\,62 \times 10^{5}$
12	$-8.137\,02 \times 10^{5}$	$-2.480\,81 \times 10^{6}$	$2.920\,13 \times 10^{7}$	$-4.708\,52 \times 10^{7}$
13	0.287 082	1.630 80	2.183 55	
14	$1.154\,31 \times 10^{-8}$	$-4.386\,88 \times 10^{-8}$	$6.104\,93 \times 10^{-8}$	
15	$-1.870\,03 \times 10^{-4}$	$-9.289\,77 \times 10^{-4}$	$2.907\,51 \times 10^{-3}$	
16	$1.174\,95 \times 10^{-6}$	$5.473\,69 \times 10^{-6}$	$-1.811\,76 \times 10^{-5}$	
17	$-1.669\,13 \times 10^{-9}$	$-8.087\,40 \times 10^{-9}$	$2.797\,27 \times 10^{-8}$	
18	1.004 81	$-7.436\,77 \times 10^{-2}$	$-4.652\,63 \times 10^{-2}$	
19	$5.471\,15 \times 10^{-10}$	$1.765\,98 \times 10^{-9}$	$3.162\,39 \times 10^{-9}$	
20	$2.468\,51 \times 10^{-4}$	$-1.006\,29 \times 10^{-3}$	$2.877\,62 \times 10^{-3}$	
21	$-1.998\,13 \times 10^{-6}$	$5.989\,56 \times 10^{-6}$	$-1.734\,22 \times 10^{-5}$	
22	$4.138\,89 \times 10^{-9}$	$-8.990\,12 \times 10^{-9}$	$2.568\,24 \times 10^{-8}$	

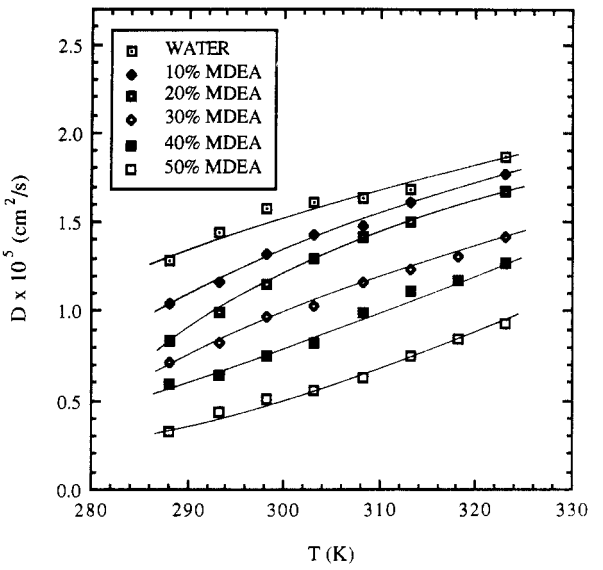

Figure 7. Diffusivity of nitrous oxide in aqueous MDEA. Lines represent the correlation.

equations are described below. Note that T is used as the main independent variable and the values of the parameters, K_i, depend only on MDEA mass fraction, w_M. The values of the K_i's may be calculated from eq 17 using the parameters given in Table IX.

Density. The experimental density measurements were correlated by

$$\rho = K_1 + K_2T + K_3T^2 \quad (9)$$

where the density, ρ, is given in g/mL and the temperature, T, in K. This equation predicts the experimental data with an average mean deviation of 0.05%. The lines in Figure 4 for the aqueous solutions correspond to the predicted values given by eq 9. It may be seen that data for pure MDEA show a lower density than for 50 wt % MDEA. This indicates the nonideality of these mixtures with a significant volume change on mixing.

Viscosity. The experimental results for the dynamic viscosity were correlated by

$$\ln \mu = K_4 + K_5/T + K_6T \quad (10)$$

where the dynamic viscosity, μ, is given in cP and the temperature, T, in K. This convenient equation correlates the experimental results with an average mean deviation of 1.1%. The lines in Figure 5 are given by eq 10.

Solubility. The solubility of N_2O in MDEA aqueous solutions obtained experimentally was correlated by

$$\ln H_{N_2O} = K_7 + \frac{K_8}{T} + \frac{K_9}{T^2} \quad (11)$$

where H_{N_2O} is given in (atm L/mol) and T in K. This equation predicts the solubility of N_2O in MDEA aqueous solutions, in the ranges of concentration and temperature specified above, with an average mean deviation of 0.32%. Equation 11 is represented in Figure 6 by the solid lines.

The solubility of CO_2 in MDEA solutions estimated from the N_2O analogy, calculated from eq 4, can be correlated by

$$\ln H_{CO_2} = K_{10} + \frac{K_{11}}{T} + \frac{K_{12}}{T^2} \quad (12)$$

This equation predicts the estimated values with an average mean deviation of 0.13%.

Diffusivity. The experimental results of N_2O diffusivity in MDEA solutions were correlated by a form of the Stokes–Einstein equation

$$D_{N_2O}\,\mu^{K_{13}}/T = K_{14} \quad (13)$$

where D_{N_2O} is in (cm^2/s), T is in K, and μ is given in g/(cm s) and was calculated by using eq 10. Equation 13 predicts the experimental data with an average mean deviation of 3.7%. The prediction of D_{N_2O} from eq 13 requires the knowledge of the solution viscosity. For more convenience, however, the same data were correlated by a simpler equation that takes into account the effect of solution viscosity implicitly. This equation has the form

$$D_{N_2O} = K_{15} + K_{16}T + K_{17}T^2 \quad (14)$$

This equation predicts the experimental data with an average mean deviation of 2.3%. The solid lines in Figure 7 represent the predicted values from eq 14.

The diffusivity of CO_2, as estimated from the N_2O analogy, was correlated by a form of the Stokes–Einstein equation

$$D_{CO_2}\,\mu^{K_{18}}/T = K_{19} \quad (15)$$

and by the simpler equation

$$D_{CO_2} = K_{20} + K_{21}T + K_{22}T^2 \quad (16)$$

Equations 15 and 16 predict the estimated values with average mean deviations of 2.9% and 2.5%, respectively.

The values of the K_i's in eq 9–16 depend on MDEA mass fraction, w_M, and are given as

$$K_i = k_{i,1} + k_{i,2}w_M + k_{i,3}w_M^2 + k_{i,4}w_M^3 \quad (17)$$

where the k_{ij} values are given in Table IX.

Acknowledgment

We gratefully acknowledge support to H.A.A. in the form of a fellowship awarded by the Kuwait Institute for Scientific Research. The MDEA for this work was provided by the Union Carbide Corporation.

Glossary

C^*_A	concentration of gas A at the gas–liquid interphase, mol/L
C°_A	concentration of gas A at the bulk liquid phase, mol/L
D_A	diffusion coefficient of gas A in amine solution, cm^2/s
D°_A	diffusion coefficient of gas A in pure water, cm^2/s
F°	concentration of MDEA in the bulk liquid phase, mol/L
g	acceleration due to gravity, cm/s^2
H_A	Henry's law constant of gas A in amine solution, L atm/mol
H°_A	Henry's law constant of gas A in pure water, L atm/mol
h	jet length, cm
$k_{i,j}$	correlation parameters in eq 17 given in Table IX
K_i	correlation parameters in eq 9–16 given by eq 17
k_2	second-order reaction rate constant, L/(mol s)
L	liquid flow rate, cm^3/s
p_A	partial pressure of species A, atm
R_A	rate of absorption of gas A, mol/s
r_s	radius of wetted sphere, cm
T	temperature, °C, K
t	contact time, s
u	velocity in θ direction over a wetted sphere, cm/s
w_M	amine mass fraction in solution

Greek Symbols

Δ_1	film thickness over a wetted sphere at the equator, cm
μ	dynamic viscosity, P

ν kinematic viscosity, cm^2/s
ρ density, g/mL

Registry No. MDEA, 105-59-9; CO_2, 124-38-9.

Literature Cited

(1) Haimour, N. K.; Bidarian, A.; Sandall, O. C. *Chem. Eng. Sci.* **1987**, *42*, 1393.
(2) Vidaurri, C.; Kahre, L. C. *Hydrocarbon Process.* **1970**, *56*, 333.
(3) Pearce, R. L.; Brownlie, T. T. *Proc. Gas Cond. Conf.* **1976**, *25th*, K-1.
(4) Goar, B. G. *Oil Gas J.* **1980**, *78*(18), 239.
(5) Daviet, G. R.; Sundermann, R.; Donnelly, S. T.; Bullin, J. A. *Hydrocarbon Process.* **1984**, *63* (May), 79.
(6) Clarke, J. K. A. *Ind. Eng. Chem. Fundam.* **1964**, *3*, 239.
(7) Weiland, R. H.; Trass, O. *Can. J. Chem. Eng.* **1971**, *49*, 767.
(8) Joosten, G. E. H.; Danckwerts, P. V. *J. Chem. Eng. Data* **1972**, *17*, 452.
(9) Sada, E.; Kumazawa, H.; Butt, M. A. *J. Chem. Eng. Data* **1977**, *22*, 277.
(10) Sada, E.; Kumazawa, H.; Butt, M. A. *J. Chem. Eng. Data* **1978**, *23*, 161.
(11) Alvarez-Fuster, C.; Midoux, N.; Laurent, A.; Charpentier, J. C. *Chem. Eng. Sci.* **1980**, *35*, 1717.
(12) Alvarez-Fuster, C.; Midoux, N.; Laurent, A.; Charpentier, J. C. *Chem. Eng. Sci.* **1981**, *36*, 1513.
(13) Laddha, S. S.; Diaz, J. M.; Danckwerts, P. V. *Chem. Eng. Sci.* **1981**, *36*, 228.
(14) Haimour, N. K.; Sandall, O. C. *Chem. Eng. Sci.* **1984**, *39*, 1791.
(15) Al-Ghawas, H. A.; Ruiz-Ibanez, G.; Sandall, O. C. *Chem. Eng. Sci.* **1989**, *44*, 631.
(16) *Chemical Engineering Handbook*, 5th ed.; McGraw-Hill: New York, 1973.
(17) *CRC Handbook of Chemistry and Physics*, 62nd ed.; CRC Press: Boca Raton, FL, 1982.
(18) *International Critical Tables of Numerical Data, Physics, Chemistry and Technology*, 1st ed.; McGraw-Hill: New York, 1928; Vol. III.
(19) Raimondi, P.; Toor, H. L. *AIChE J.* **1959**, *5*, 86.
(20) Ratcliff, G. A.; Holdcroft, J. G. *Trans. Inst. Chem. Eng.* **1963**, *41*, 315.
(21) Vivian, J. E.; King, C. J. *AIChE J.* **1964**, *10*, 220.
(22) Thomas, W. J.; Adams, M. J. *Trans. Faraday Soc.* **1965**, *61*, 668.
(23) Perez, J. F.; Sandall, O. C. *AIChE J.* **1973**, *20*, 770.
(24) Tang, A.; Sandall, O. C. *J. Chem. Eng. Data* **1985**, *30*, 189.
(25) Davidson, J. F.; Cullen, E. J. *Trans. Inst. Chem. Eng.* **1957**, *35*, 51.
(26) Olbrich, W. E.; Wild, J. D. *Chem. Eng. Sci.* **1969**, *24*, 25.
(27) Goettler, L. A. Ph.D. Thesis, University of Delaware, Newark, 1967.
(28) Wild, J. D.; Potter, O. E. *Chem. Eng. J.* **1972**, *4*, 69.
(29) Tomcej, R. A.; Lal, D.; Ranwala, H. A.; Otto, F. D. *Presented* at the AIChE Meeting, Miami, Nov 2-7, 1986.

Received for review June 15, 1986. Revised February 28, 1989. Accepted May 26, 1989.

High-Pressure Binary Phase Equilibria of Aromatic Hydrocarbons with CO_2 and C_2H_6

Choon-Ho Kim, Angela B. Clark, P. Vimalchand, and Marc D. Donohue*

Department of Chemical Engineering, The Johns Hopkins University, Baltimore, Maryland 21218

High-pressure vapor-liquid equilibria of several binary systems containing aromatic hydrocarbons as one component and supercritical carbon dioxide or ethane as the other component were measured by using a dynamic system in which both vapor and liquid phases were circulated. The aromatic hydrocarbons that were used in this study are anisole, benzaldehyde, tetralin, and 1-methylnaphthalene. The phase equilibria of binary systems containing carbon dioxide were measured at two different temperatures, 343 and 373 K, and pressures up to 22 MPa. For ethane binary systems, equilibrium measurements were made at 373 K and pressures up to 12 MPa. In addition to measuring temperature, pressure, and phase compositions, the vapor- and liquid-phase densities also were determined for both carbon dioxide and ethane binary systems.

Introduction

Although considerable phase equilibrium data are available for low molecular weight aliphatic hydrocarbons encountered in natural gas and oil industries, such data are scarce for high molecular weight hydrocarbons, especially aromatic hydrocarbons. High-pressure phase equilibrium data of systems containing aromatic hydrocarbons are necessary for design and operation of coal processing plants and for selective extraction of valuable chemicals from liquefied coal mixtures using a supercritical fluid solvent. In this study, we have measured binary phase equilibria of systems containing aromatic hydrocarbons (anisole, benzaldehyde, tetralin, and 1-methylnaphthalene) as one of the components and a supercritical fluid (carbon dioxide and ethane) as the other component.

The vapor-liquid equilibria of the system carbon dioxide-tetralin was measured since tetralin is present in significant amounts in many liquefied coal mixtures. Only limited data are available for this system. Experimental data for binaries of carbon dioxide with tetralin and 1-methylnaphthalene are available (*1*, *2*) at very high temperatures (462-704 K) and pressures only up to 5 MPa. Experimental data for the system carbon dioxide-1-methylnaphthalene are also reported by Morris and Donohue (*3*), who measured at two different temperatures, 353.15 and 413.15 K, and pressures up to 14.4 MPa. Limited experimental data are reported in literature for the carbon dioxide-benzaldehyde system (ambient pressure and temperatures ranging from 291 to 309 K) by Kunnerth (*4*). No literature data is available for the carbon dioxide-anisole system. Again, for ethane-anisole and ethane-benzaldehyde binary systems, phase equilibrium data are not available in literature. Only Henry's constant (*5*) and limited solubility data (*6*) are available for the ethane-1-methylnaphthalene system.

In order to measure the phase equilibria of systems containing high-pressure carbon dioxide or ethane as one of the components, we built an equilibrium apparatus that circulates both the vapor and liquid phases. This experimental system provides a rapid and reproducible means of obtaining phase equilibrium data. In addition to measuring the temperature, pressure, and vapor- and liquid-phase compositions, we also measured the vapor- and liquid-phase densities. Although density data are readily available for pure compounds, few density measurements for mixtures are reported in literature. For carbon dioxide systems, the equilibrium phase compositions and liquid and vapor densities of the mixtures were measured at two temperatures and various pressures ranging from 3 to 22 MPa. For binary systems containing ethane, the measurements were made at 373 K and pressures up to 12 MPa. The

0021-9568/89/1734-0391$01.50/0